Versão do arquivo anexado / Version of attached file:

Versão do Editor / Published Version

Mais informações no site da editora / Further information on publisher's website:

https://pubs.acs.org/doi/10.1021/acs.energyfuels.0c02786

DOI: 10.1021/acs.energyfuels.0c02786

Direitos autorais / Publisher's copyright statement:

Article

CO$_2$ Gasification of Sugarcane Bagasse Char: Consideration of Pyrolysis Temperature, Silicon and Aluminum Contents, and Potassium Addition for Recirculation of Char

Ingrid Lopes Motta, Ross A. Arnold, Francisco Javier Lopez-Tenllado, Rubens Maciel Filho, Maria Regina Wolf Maciel, and Josephine M. Hill*

Read Online

ACCESS | Metrics & More | Article Recommendations | SI Supporting Information

ABSTRACT: In sugarcane bagasse gasification, char recirculation to the gasifier improves the syngas quality and process efficiency. To determine the effect of char properties on the reaction kinetics, in this work, the pregasification pyrolysis temperature, particle size, and catalyst (potassium) loading were varied. Char samples were prepared at 750−900 °C via pyrolysis and gasified isothermally in a thermogravimetric analysis unit at 850 °C with CO$_2$, and gasification data were modeled using the random pore and extended random pore models. Increasing pyrolysis temperatures did not affect the char morphology and surface composition but did reduce the surface area, as determined by N$_2$ adsorption, decreasing initial gasification rates, and the overall fitted rate constants. Reduction of the particle size via ball milling decreased the time required for complete conversion and changed the shape of the rate versus conversion curves from monotonically decreasing to concave down. The char sample prepared via pyrolysis at 900 °C was an exception, having a maximum rate at ∼10% conversion without ball milling. After ball milling of the char sample prepared at 750 °C, there was an accumulation of ash (Al and Si) on the surface of the particles and a reduction in the surface area, consistent with the ash blocking pores—the porosity in these samples increased during the initial stages (up to ∼20% conversion) of gasification. The gasification behavior was generally well modeled by the extended random pore model. Although the addition of KOH (K/Al mass ratio ∼ 0.2−1.25) enhanced the gasification rates, too much K—from the addition of KOH or after 90% conversion—created mass-transfer limitations resulting in lower gasification rates.

1. INTRODUCTION

Sugarcane bagasse (SCB) is the solid residue of the juice extracted from sugarcane,[1] with approximately 300 kg of SCB produced for every tonne of sugarcane processed.[2] Despite the low cost and high availability, SCB is usually underused in low-added-value applications such as heat and power production in cogeneration plants.[3] An alternative use for SCB is as a feedstock for gasification processes. Although the majority of the carbon feed will be converted to gaseous and liquid products (85−95 wt % from 720−840 °C in industrial circulating fluidized bed gasifiers),[4] some solid residue will remain. This residue, referred to as char (or as biochar because it was obtained from biomass), can be used in various applications, such as in soil remediation, carbon sequestration, and wastewater treatment,[5,6] but can also be recirculated in the gasifier to improve the cold gas efficiency of the reactor and increase the syngas heating value.[7] The char properties depend on the gasifier conditions (e.g., temperature and catalyst) and may affect gasification rates during recirculation.

Previous gasification studies of SCB char[8−12] were performed under nonisothermal conditions that are dissimilar to the conditions within circulating fluidized bed gasifiers. Nonetheless, the authors of these studies suggested that temperatures above 800 °C removed the hydroxyl, aliphatic C−H, and olefinic C=C groups, and that increasing pyrolysis temperatures affected the char physical structure such that the reactivity was reduced.[9,10] Char reactivity generally increases

with the surface area (i.e., increased contact between gasifying agents and carbon sites)[13] and, for the biochar materials studied thus far (e.g., oak, pine, grass,[14] soybean stover, peanut shell,[15] pig manure, wheat straw,[16] *Douglas fir*, and hazelnut shell[17]), maximum surface areas were achieved up to a pyrolysis temperature of ∼700 °C.[14−17] Specific surface areas on a per mass basis are also a function of particle size. Within the laboratory, particles can be ball-milled to reduce their size, and previous studies in which SCB char was ball milled focused on their use in adsorption applications,[18−20] as precursors for carbon electrodes,[21] and as polymer composites.[22] The milling reduced the particle size of SCB char from above 100 μm to 100−500 nm,[18,19,22] increased the char surface area from 51 to 331 m^2/g for char samples prepared at 450 °C,[19,20] and added oxygen functional groups to the surface by creating open ends of the carbon chains which are exposed to the atmosphere,[19,20] which may improve the char gasification performance.

Alkali metals such as potassium participate in the oxygen-transfer cycle and catalyze gasification.[23] Potassium is mobile

within and between particles, but this mobility can be hindered by the presence of elements other than carbon. For example, Si and Al deactivate K through the formation of aluminosilicate species (e.g., $KAlSiO_4$).[24] Al is typically present in lower amounts than Si in gasification feeds, and thus, Al is the limiting reactant in potassium aluminosilicate formation. Feedstocks usually require K/Al ratios higher than 0.5[25,26] or the addition of alkaline earth species such as Ca that preferentially reacts with Si and Al[25] to ensure that there is sufficient K to catalyze the gasification. SCB contains 1.3 wt % SiO_2, 0.2 wt % Al_2O_3, and 0.4 wt % CaO (calculated based on the SCB ash content and ash elemental composition),[1] so the appropriate catalytic amount of potassium has to be determined.

The current study was undertaken to determine how the pyrolysis temperature above 700 °C, char particle size, Si and Al contents, and K addition affect the gasification rates of SCB char under isothermal conditions. The char samples were prepared via pyrolysis at different temperatures (750, 800, 850, or 900 °C) and gasified at 850 °C with CO_2 in a thermogravimetric analysis unit. Some of the char samples were ball milled before gasification, with or without KOH, aiming to reduce the particle size, increase the surface area, and reduce mass-transfer limitations. In char samples with added KOH, ball milling was performed to improve K dispersion. Kinetic modeling and model discrimination techniques were used to quantitatively relate the gasification performance to the physical and chemical properties of the char samples.

2. EXPERIMENTAL SECTION

2.1. Sugarcane Bagasse Collection and Characterization. SCB samples were collected from the sugar mill USJ in Araras (São Paulo, Brazil) in April 2019, dried (to reduce the moisture content from 60 to 6 wt %), and sieved using Tyler test sieves. Proximate analysis was performed via macrothermogravimetric analysis (TGA) as per ASTM D7582 in an automatic multiple sample thermogravimetric analyzer TGA-1000 (Navas Instruments, Conway, USA) with approximately 500 mg of each sample. Ultimate analysis was conducted via CHNOS chemical analyses in a Vario Macro Cube analyzer (Elementar, Hanau, Germany) with ~80 mg of sample that was placed onto a tin sheet, molded into a capsule, and then combusted at 1150 °C. The produced gases (N_2, CO_2, H_2O, and SO_2) were quantified by gas chromatography with a thermal conductivity detector (GC-TCD).

For scanning electron microscopy (SEM) analysis, samples were transferred to a double-sided carbon tape fixed to stubs and sputter-coated in a coating system model K450 (EMITECH, Kent, United Kingdom) with gold (20 nm film) under vacuum for 2 min. The samples were analyzed in an SEM model Leo 440i (LEO Electron Microscopy, Cambridge, United Kingdom) with an energy-dispersive X-ray (EDX) detector (Cambridge, United Kingdom) for measurements at 20 kV and 100 mA (SEM imaging) or 800 mA (EDX analysis). In addition to observing the sample morphology, particle size distributions were calculated from the SEM images by measuring at least 200 particles. EDX analysis was used to map at least five different regions to obtain average elemental compositions from which the K/Al and K/C ratios on the char surfaces were calculated. K/Al and K/C ratios were analyzed because K is the most active species for gasification, Al is the limiting reactant in the formation of potassium aluminosilicate, and C is the substrate to undergo gasification. The standard deviations of the compositions are reported (Table 1 and Table 2).

2.2. Char Preparation and Characterization. Char samples were prepared via pyrolysis in a quartz reactor (ID = 25 mm) placed in a furnace (Mellen, Concord, USA) and connected to a scrubber containing methoxy propanol and water to trap any tar or syngas

Table 1. Proximate and Ultimate Analyses of SCB

proximate analysis (wt %)	
moisture content	6.5 ± 0.1
volatile matter (db[a])	73.5 ± 1.4
fixed carbon (db)	16.9 ± 0.9
Ash (db)	9.6 ± 0.8
ultimate analysis (wt %, db)	
C	41.3 ± 0.3
H	6.4 ± 0.1
O[b]	41.9 ± 0.3
N	0.6 ± 0.0
S	0.2 ± 0.1
Ash	9.6 ± 0.8

[a]db—dry basis. [b]Oxygen content was calculated by difference.

produced. Approximately, 4 g of SCB was heated at 25 °C min^{-1} in flowing N_2 (185 mL min^{-1}) to the desired temperature (750, 800, 850, or 900 °C). The pyrolysis temperatures were selected based on the typical temperature ranges of circulating fluidized bed gasifiers. The sample was maintained at the pyrolysis temperature for 2 h before being cooled to room temperature. The char preparation yield, Y, was determined by eq 1, where m_f and m_0 refer to the final and initial masses, respectively.

$$Y = \frac{m_f}{m_0} \tag{1}$$

A portion of each char sample was ball milled in a Pulverisette 6 Planetary Mono Mill (Fritsch, Idar-Oberstein, Germany) for 3 h at 500 rpm with zirconia balls of 5 mm diameter. The rotation direction was altered every 30 min to increase homogenization. The char sample prepared at 750 °C was ball milled without KOH (K/Al = 0.2 [molar basis]; KOH loading: 0 wt %) and with different amounts of KOH (K/Al = 0.5, 1.0, and 1.25; KOH loadings: 19, 53, and 70 wt %, respectively). The char samples were named according to the pyrolysis temperature (e.g., char750 refers to a sample prepared at 750 °C). The char samples after ball milling have the prefix "BM" and, if the sample was ball milled with KOH, its target molar K/Al ratio is indicated (e.g., BM-char750 with K/Al = 0.5 refers to a sample pyrolyzed at 750 °C and then ball milled with KOH at a target K/Al molar ratio of 0.5).

All char samples were analyzed with N_2 and CO_2 adsorption to determine their surface area, micropore volume, and pore size distribution. First, the samples were degassed using a sample degas system VacPrep 061 (Micromeritics, Norcross, USA) under a vacuum of 100 μm Hg (13.3 Pa) at 200 °C for 18 h. The samples were then transferred to the adsorption analyzer Tristar II Plus (Micromeritics, Norcross, USA) for N_2 adsorption analysis at −196 °C, followed by CO_2 adsorption at 0 °C. The surface areas were determined with SAIEUS software (Micromeritics, Norcross, USA) using the two-dimensional nonlocal density-functional theory (2D-NLDFT) fitted with N_2 and CO_2 adsorption data and λ values of 2.0−3.0, as well as with the BET equation using N_2 adsorption results. N_2 and CO_2 adsorption data were also used to obtain pore size distributions via 2D-NLDFT, and CO_2 adsorption data were used to calculate micropore volumes with the Dubinin−Radushkevich equation.

The surface functional groups of four char samples (char prepared at 750 and 850 °C, both prior to and following ball milling) were determined with a Fourier-transform infrared spectrometer (Nicolet iS50, Thermo Scientific, USA) with an attenuated transmission reflectance (ATR) attachment. ATR spectra were collected in the 4000 to 400 cm^{-1} wavenumber range, accumulating 32 scans at 2 cm^{-1} resolution.

Ash contents were determined as per ASTM D3174 in an SDT Q600 thermogravimetric analyzer (TA Instruments, New Castle, USA). The SEM−EDX analyses of the char samples followed similar protocols to those used for the SCB samples except that a different instrument was used (Phenom ProX instrument, Thermo-Fisher, 15

Table 2. Estimated Surface Composition of SCB and Char (as-Prepared at 750 and 850 °C and after Ball Milling), as Determined by EDX Analysis

element (mol %)	SCB	char750	char850	BM-char750	BM-char850
C	53.0 ± 2.0	86.5 ± 1.9	86.9 ± 2.5	64.8 ± 1.0	65.1 ± 1.7
O	46.2 ± 2.1	10.9 ± 1.5	10.8 ± 1.4	26.6 ± 1.8	27.0 ± 2.6
Si	0.4 ± 0.3	1.4 ± 0.8	0.7 ± 0.4	6.1 ± 0.6	5.1 ± 1.0
Al	0.2 ± 0.1	0.7 ± 0.2	0.6 ± 0.3	1.2 ± 0.1	1.0 ± 0.2
K	0.1 ± 0.0	0.2 ± 0.0	0.4 ± 0.3	0.3 ± 0.1	0.2 ± 0.0
Ca	0.02 ± 0.02	0.1 ± 0.0	0.2 ± 0.2	n.d.[a]	n.d.
Mg	n.d.	0.1 ± 0.1	0.2 ± 0.1	0.1 ± 0.0	0.1 ± 0.0
K/Al	0.4 ± 0.1	0.3 ± 0.1	0.7 ± 0.4	0.2 ± 0.1	0.2 ± 0.0
K/C	0.001	0.002	0.004	0.004	0.002

[a]n.d.: not detected. Individual measurements and elemental composition in wt % are provided in Supporting Information A.

kV, Eindhoven, Netherlands), and the samples were not sputter-coated before analysis.

All samples were stored under ambient conditions between char preparation via pyrolysis and gasification tests. As sample devolatilization is complete by 600 °C[27] and pyrolysis was performed at a minimum temperature of 700 °C, sample storage did not further affect the volatile content of char.

2.3. Gasification Experiments. Gasification experiments were conducted in a benchtop TGA instrument (SDT Q600, TA Instruments, New Castle, USA) with 3.5 mg of sample in an alumina crucible. Each experiment consisted of heating to the gasification temperature (850 °C) under an inert N_2 atmosphere (200 mL min^{-1}) with a heating rate of 20 °C min^{-1}. Once the system reached 850 °C, isothermal char gasification proceeded with a CO_2 flow of 200 mL min^{-1} and a N_2 flow of 5 mL min^{-1} to prevent backflow of CO_2 over the TGA balance. The gasification temperature of 850 °C is within the operating range of fluidized and fixed bed gasifiers (750−950 °C). Gasification rates with CO_2 are similar to those with steam, as shown in previous studies on petcoke and SCB co-gasification under CO_2[8] and steam[28] atmospheres.

The TGA data for gasification were analyzed and treated as follows: the time, t, versus mass, m, data were smoothed to 1000 points using the locally estimated scatterplot smoothing (LOESS) technique in SigmaPlot 14.0 with a polynomial order of 3 and weighted according to 5% of the neighboring data. The reduced data were used to calculate several kinetic parameters. The sample and carbon conversions in the gasification stage were calculated using eqs 2 and 3, respectively, where the subscripts 0, t, and f denote the sample mass at time zero, time t, and at the end of the experiment, respectively. The carbon reaction rates were calculated by eq 4 using numerical integration, where the subscripts 1 and 2 denote two consecutive time points that are 1 s apart, while ash denotes the mass fraction of ash in the sample.

$$X_{sample} = \frac{m_{sample,0} - m_{sample,t}}{m_{sample,0} - m_{sample,f}} \quad (2)$$

$$X_{carbon} = \frac{X_{sample}}{1 - ash} \quad (3)$$

$$\frac{dX_{carbon}}{dt}(t_1) = \frac{X_2 - X_1}{t_2 - t_1} \quad (4)$$

2.4. Kinetic Modeling and Model Discrimination. The gasification data were modeled using the random pore model (RPM, eq 5)[13] and the extended random pore model (eRPM, eq 6).[29]

$$\frac{dX}{dt} = k_j(1 - X)\sqrt{1 - \psi \ln(1 - X)} \quad (5)$$

$$\frac{dX}{dt} = k_j(1 - X)\sqrt{1 - \psi \ln(1 - X)}[1 + c(1 - X)^p] \quad (6)$$

In eqs 5 and 6, k_j is the rate constant, ψ is the structural factor,[13] and c and p are two semiempirical parameters.[29] During gasification,

pores develop within the carbon structure, increasing the surface area. The developed pores collapse as gasification proceeds, reducing the surface area. The structural factor ψ represents the difference between the initial and maximum surface areas during gasification.[13] The parameters c and p relate to the value and position of the maximum gasification rate, respectively, yielding a better fit of the mathematical model.[29] Athena Visual Studio v14.2 was used in the kinetic modeling and model discrimination.

In the kinetic modeling, k_j, ψ, c, and p were determined using the nonlinear least-squares method. The RPM and eRPM were fit to the gasification rates (dX_{carbon}/dt) as a function of carbon conversion (X_{carbon}) by minimization of the residual sum of squares (RSS) with an experimental error of 10%. The modeling required data with equally spaced conversions to avoid the over-representation of data points at high-conversion levels and allow a better fit.[30] The model discrimination was performed using the Akaike information criterion (AIC), defined in eq 7, where m is the number of estimated parameters, n is the number of observations (1000 for both models), and RSS is the residual sum of squares. The models were also compared with the calculation of the Akaike probability share (π_{AIC}), shown in eq 8, where L_k is the relative likelihood of model k, which is defined by eq 9.

$$AIC = m\frac{2}{n} + \ln\left(\frac{1}{n}RSS\right) \quad (7)$$

$$\pi_{AIC} = \frac{L_k}{\sum_{i=1}^{k} L_k} \quad (8)$$

$$L_k = \exp\left(\frac{AIC_{min} - AIC_k}{2}\right) \quad (9)$$

3. RESULTS AND DISCUSSION

The proximate and ultimate analyses of SCB are given in Table 1. The volatile matter and fixed carbon contents were 73.5 and 16.9 wt % on a dry basis (db), respectively, with both carbon and oxygen contents of ∼41 wt % (db), as reported elsewhere.[1] The ash content of 9.6 wt % (db) was higher than the values previously reported in the literature for SCB (2.0−7.4 wt %),[1,31] but this value has been shown to be dependent on the technique used for the extraction of juice.[1] The SCB ash content was also higher than that of other biomass sources such as switchgrass (6.3 wt %),[25] wheat straw (1.8−3.6 wt %), and corn stover (2.0 wt %).[32] SCB had low nitrogen (0.6 wt %, db) and sulfur (0.2 wt %, db) contents, which is beneficial for thermochemical processes in which these species are converted to pollutants including SO_x, NO_x, and so forth.[33] The ash mainly contained Si, Al, K, Ca, and Mg. Low levels of Fe (<1.0 mol %) and Ti (<0.1 mol %) were also detected; rather than being part of the sugarcane structure, however, Fe and Ti
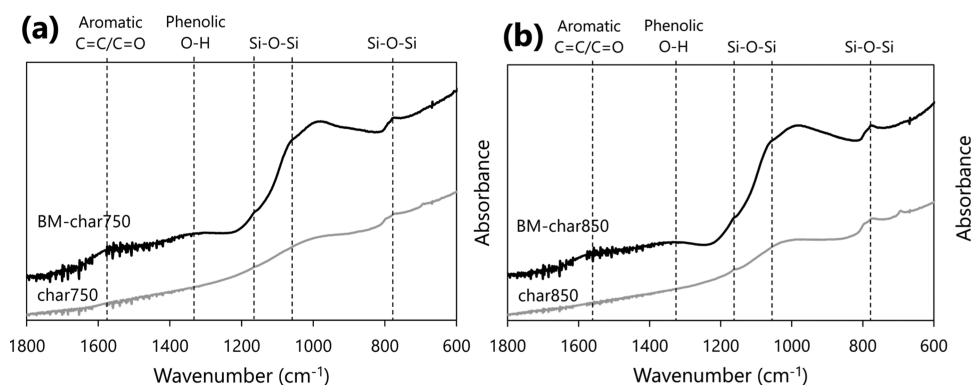
Figure 1. FTIR spectra of SCB char produced at (a) 750 °C and (b) 850 °C, as-prepared and ball milled.
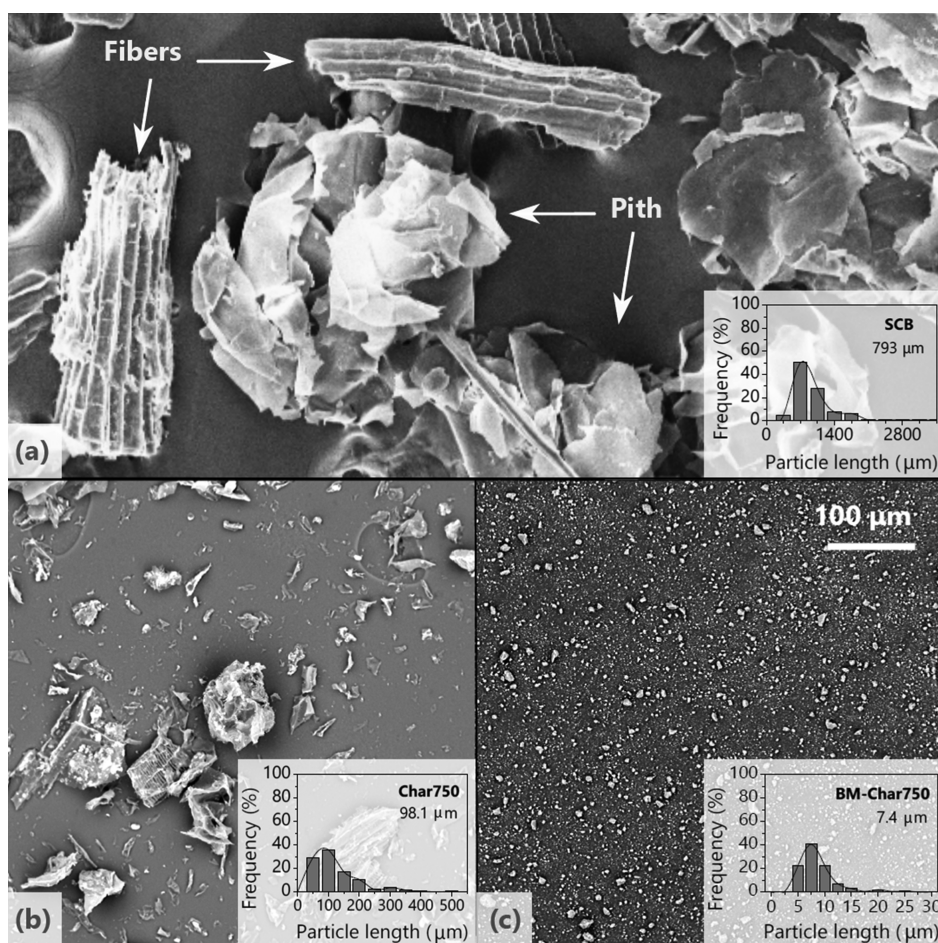
Figure 2. SEM images and particle size distributions of (a) SCB, (b) SCB char as-prepared at 750 °C, and (c) SCB char prepared at 750 °C and ball milled. The scale bar applies to all images.

originated from the soil and the biomass grinder,[22] respectively.

Although the char devolatilization extent depends on the temperature and time, devolatilization is generally complete by 600 °C.[27] The recirculated char in a gasifier will be exposed to temperatures of 750–900 °C, and so the SCB char was produced at these temperatures. All char samples had an overall mass loss of ∼75 wt % and a final ash content of ∼35 wt % (db). The elemental compositions of SCB and char samples were estimated by SEM−EDX, and the results are shown in Table 2. For SEM−EDX analysis, the beam penetration depth is only a few nanometers and detection of light elements is limited (due to matrix and absorption effects). Therefore, the EDX elemental determinations of C and O (Table 2) are only estimates of the sample surface and are not expected to the be the same as the bulk analysis done via ultimate analysis (Table 1).

No significant differences in surface composition were observed between samples produced at different pyrolysis temperatures. The lower oxygen and higher carbon contents of char in comparison to those of SCB are a result of the loss of volatile matter. After ball milling, the compositions of the char samples changed again (Table 2). Both the oxygen and silicon contents increased significantly, from 11 to 27 mol % and from
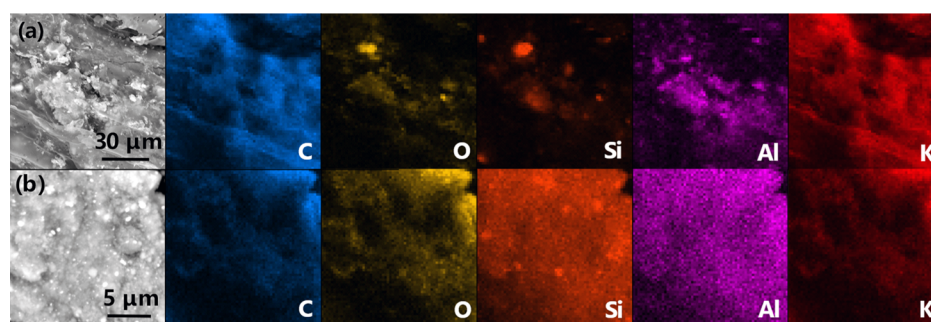
Figure 3. EDX mapping results of (a) SCB char as-prepared at 750 °C and (b) after ball milling.

Table 3. N$_2$ and CO$_2$ Adsorption Results of SCB Char as-Prepared and After Ball Milling

	surface area (m^2/g)			micropore volume (cm^3/g)	pore width (nm)
sample	2D-NLDFT N$_2$	BET N$_2$	2D-NDLFT CO$_2$	DR CO$_2$	2D-NDLFT CO$_2$
char750	294	210	446	0.14	0.47
char800	257	182	406	0.12	0.47
char850	216	372	482	0.13	0.46
char900	79	62	403	0.12	0.46
BM-char750	94	89	189	0.05	0.42
BM-char800	104	96	230	0.05	0.46
BM-char850	172	137	235	0.06	0.46
BM-char900	71	68	123	0.03	0.44
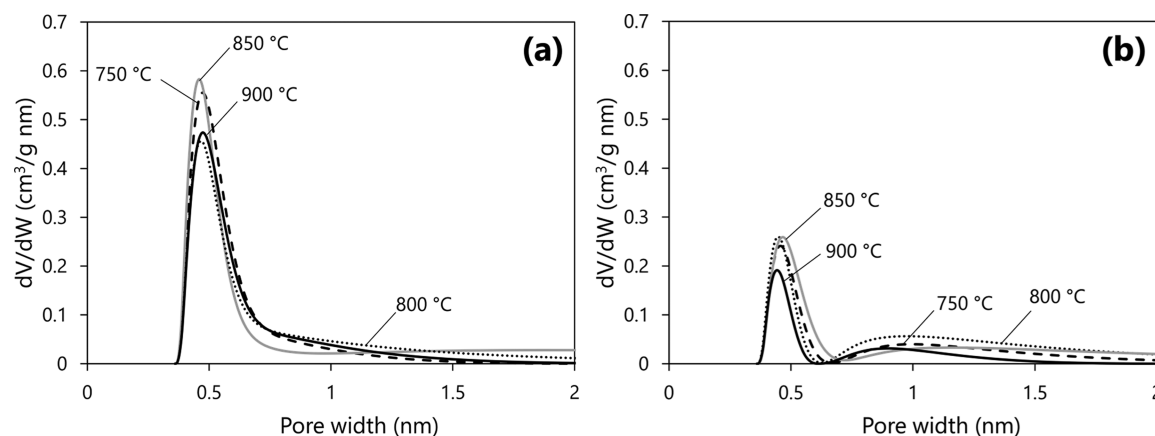
Figure 4. Pore size distributions determined via 2D-NLDFT calculations with CO$_2$ adsorption data of char samples (a) as-prepared and (b) after ball milling.

~1 to 5−6 mol %, respectively, while the aluminum content increased slightly (~0.7 to 1.1 mol %). Higher Si contents (i.e., increased Si−O−Si signals) were also observed in the FTIR spectra (Figure 1) after ball milling.[34] The peaks for aromatic C=C/C=O and phenolic O−H also increased after ball milling, in agreement with previous studies.[19,21] It can be noted that no functional groups were observed in the region of 1800−4000 cm^{-1} in the FTIR spectra.

SCB had a heterogeneous morphology (Figure 2a) with two main particle groups: fibers, which were long (hundreds of microns) particles composed of lignified cell wall layers, and the pith, which were smaller less dense spherical particles.[1,35] The pyrolysis process did not change the biomass morphology (Figure 2b, fiber and pith remained), as has also been observed for poplar char,[36] but reduced the average particle size from 793 to 100 μm. The image in Figure 2b is of a char sample prepared at 750 °C, but all the char samples had similar morphologies and size distributions, regardless of the pyrolysis

temperature (i.e., 750−900 °C). Ball milling reduced the char particle size further to less than 10 μm (Figure 2c, which is representative of all the ball-milled char samples), and the fiber and pith were indistinguishable.

Figure 3 shows the EDX mapping results of SCB char particles (note the difference in scale bars, which reflects different particle sizes) prepared at 750 °C before and after ball milling. While C and K are uniformly distributed on all samples, O, Al, and Si are initially observed in isolated areas, which then get well-dispersed and become much more prominent after ball milling (note the images are representative of five particles per sample mapped and all char samples). A previous study that used ball-milled SCB char as a substitute for carbon black in polymeric composite applications observed dispersed Si agglomerates in micro-X-ray tomography and SEM analyses, which were assumed to come from the SCB char.[22] The ash species are harder than the carbon substrate (for instance, char samples have hardness values of 0.1−5.0
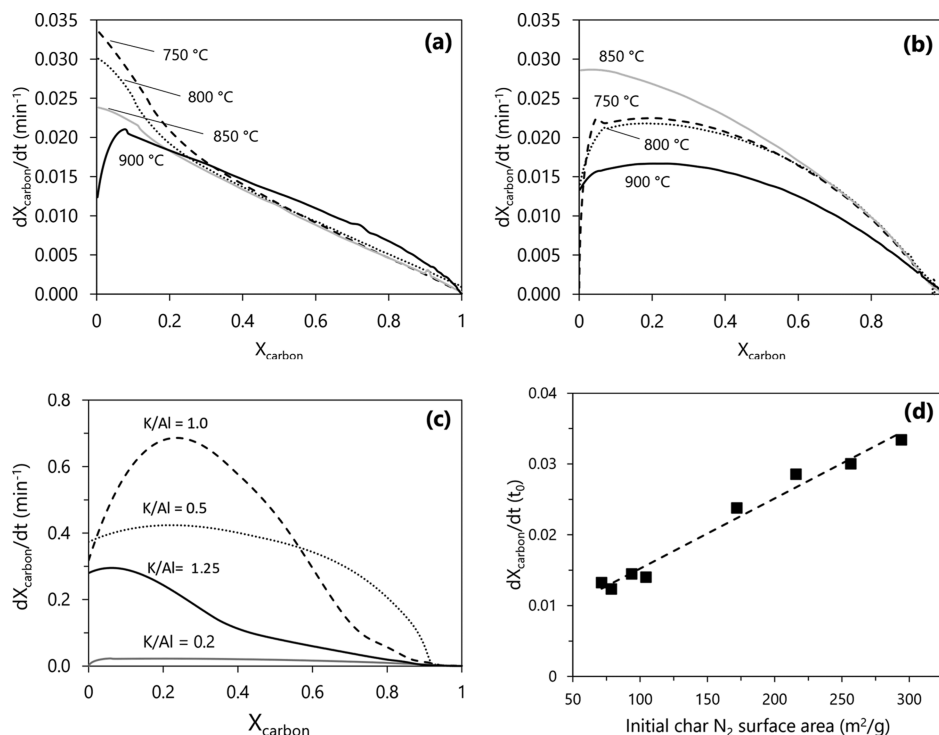
Figure 5. CO_2 gasification rates at 850 °C as a function of carbon conversion for SCB char: (a) as-prepared, (b) after ball milling, and (c) after ball milling with different KOH loadings. (d) Initial carbon conversion rates as a function of initial char surface area (before gasification) for char samples as-prepared and ball milled without KOH. In (a,b), the labels on the curves refer to the pyrolysis temperatures used to prepare the samples. In (c), the char samples were prepared at 750 °C and then ball milled with various amounts of KOH (the curve for K/Al = 0.2 corresponds to the char with no additional K, BM-char750). In (d), the surface areas were determined using N_2 adsorption (2D-NLDFT N_2 values in Table 3).

GPa,[37−40] while SiO_2, one of the main species of char samples in the current study, has hardness values of ∼11 GPa).[41]

The surface areas, pore volumes, and pore size distributions of char samples were determined using N_2 and CO_2 adsorption data, and the results are given in Table 3 and Figure 4. The BET model is generally not suitable for microporous materials,[42] but the values are included for comparison with the literature. The surface areas measured by N_2 adsorption (and fit by the 2D-NLDFT model) decreased from 294 to 79 m^2/g as the pyrolysis temperature increased from 750 to 900 °C, indicating that higher pyrolysis temperatures lead to the partial collapse of the char structure. This result is consistent with the maximum surface areas being achieved at pyrolysis temperatures at or below 700 °C for other biochar materials.[14−17] For example, a study of the effect of pyrolysis temperature on the physical characteristics of the safflower seed press cake—a cake obtained from the cold-press extraction of safflower seeds which, therefore, has a different structure than SCB—indicated that the BET surface area decreased above a pyrolysis temperature of 700 °C.[43] Pyrolysis temperatures lower than 750 °C were not used because recirculated particles in a fluidized bed gasifier will have experienced temperatures of at least 750 °C. There was not a trend in the surface areas measured by CO_2, which probes the ultramicropores (<0.7 nm), with the surface areas varying between 403 (char900) and 482 m^2/g (char850). Pyrolysis reduces the microporosity of char but has a negligible effect on ultramicroporosity. The micropore volumes and average pore widths determined with 2D-NLDFT calculations using CO_2 adsorption data were similar for all samples (∼0.13 cm^3/g and 0.46 nm, respectively).

After ball milling, there was a significant decrease in the number of ultramicropores (i.e., CO_2 uptake), as evidenced by the lower micropore volumes in Table 3 and the normalized adsorption curves using the Dubinin−Radushkevich equation in Supporting Information B. Also, ball milling significantly reduced the surface areas determined by N_2 adsorption (and fit by the 2D-NLDFT model) for the char samples prepared at 750 and 800 °C (294 to 94 and 257 to 104 m^2/g, respectively); there were smaller decreases in surface area for the samples prepared at 850 °C (216 to 172 m^2/g) and 900 °C (79 to 71 m^2/g). In contrast to pyrolysis, ball milling reduced microporosity and ultramicroporosity, possibly due to the accumulation of Si/SiO_2 at the surface of the particles blocking pores. The pore size distributions (Figure 4) reflect these changes after ball milling. In other ball milling studies with SCB char, the samples were prepared at 600 °C,[19,21] and their surface areas did not significantly change after ball milling (359 and 364 m^2/g for unmilled and milled char, respectively, as determined by N_2 adsorption). As mentioned earlier, the physical properties depend on the pyrolysis temperature, and so these studies cannot be directly compared with the results obtained herein. Of note, the pore size distributions determined from the N_2 adsorption data and fitted with the 2D-NLDFT model are given in Figure B.2 (Supporting Information B). As there were only one or two data points for pore widths above 2 nm, the pore size distributions with N_2 adsorption data are likely inaccurate for most of the samples.

Isothermal gasification of the char samples was carried out at 850 °C with CO_2, and carbon conversion rates as a function of conversion are shown in Figure 5 for the char samples. For the as-prepared samples (Figure 5a), the rates of gasification decreased with the pyrolysis temperature up to ∼20%

Table 4. Initial K/Al Ratios Estimated by EDX and Time Required for 50% ($t_{0.5}$) and 90% ($t_{0.9}$) Carbon Conversion for SCB Char Samples Gasified with CO_2 at 850 °C

sample	KOH loading (wt %)	K/Al		K/C		$t_{0.5}$ (min)	$t_{0.9}$ (min)
		target	EDX	target	EDX		
			BM-char750 with[a]				
K/Al = 0.2[b]	0	0.2	0.2	0.004	0.004	24	60
K/Al = 0.5	19	0.5	2.4	0.009	0.028	1.2	3
K/Al = 1.0	53	1.0	15	0.018	0.13	0.9	7
K/Al = 1.25	70	1.25	43	0.023	0.41	3.0	21

[a]K/Al ratios of 0.2, 0.5, 1.0, and 1.25 correspond to KOH loadings of 0, 19, 35, and 70 wt %, respectively. [b]Same sample as BM-char750.

Table 5. Rate Constants (k_j), Structural Factors (ψ), and Empirical Parameters (c and p) of the SCB Char Samples with and without Added K, Calculated via the RPM and eRPM

sample	RPM			eRPM			
	R^2	k_j (min^{-1})[a]	Ψ	R^2	Ψ	c	p
char750	0.972	$2.6 \cdot 10^{-2} \pm 1.1 10^{-4}$	0 ± 0	0.994	0 ± 0	0.45 ± 0.01	8.9 ± 0.3
char800	0.974	$2.5 \cdot 10^{-2} \pm 8.7 \cdot 10^{-5}$	0 ± 0	0.986	0 ± 0	0.32 ± 0.05	12.9 ± 0.9
char850	0.996	$2.3 \cdot 10^{-2} \pm 3.4 \cdot 10^{-5}$	0 ± 0	0.998	0.07 ± 0.00	0.13 ± 0.05	5.6 ± 0.3
char900	0.991	$2.0 \cdot 10^{-2} \pm 8.6 \cdot 10^{-5}$	1.21 ± 0.03	0.996	1.22 ± 0.01	-0.46 ± 0.02	69.9 ± 4.2
BM-char750[c]	0.962	$1.9 \cdot 10^{-2} \pm 2.4 \cdot 10^{-4}$	4.07 ± 0.16	0.985	3.92 ± 0.04	-0.92 ± 0.03	120.1 ± 8.3
BM-char800	0.990	$2.0 \cdot 10^{-2} \pm 1.5 \cdot 10^{-5}$	3.49 ± 0.07	0.993	3.36 ± 0.02	-0.35 ± 0.02	48.6 ± 4.9
BM-char850	0.996	$3.0 \cdot 10^{-2} \pm 7.5 \cdot 10^{-5}$	0.73 ± 0.01	0.997	0.71 ± 0.01	-0.05 ± 0.01	12.0 ± 3.2
BM-char900	0.991	$1.5 \cdot 10^{-2} \pm 4.6 \cdot 10^{-5}$	3.40 ± 0.04	0.993	3.42 ± 0.01	-0.15 ± 0.01	47.2 ± 4.7
			BM-char750 with[b]				
K/Al = 0.2[c]	0.962	$1.9 \cdot 10^{-2} \pm 2.4 \cdot 10^{-4}$	4.07 ± 0.16	0.985	3.92 ± 0.04	-0.92 ± 0.03	120.1 ± 8.3
K/Al = 0.5	0.969	$3.8 \cdot 10^{-1} \pm 2.3 \cdot 10^{-3}$	4.02 ± 0.08	0.969	4.02 ± 0.03	-0.03 ± 0.02	21.5 ± 18.7
K/Al = 1.0	0.783	$6.8 \cdot 10^{-1} \pm 9.7 \cdot 10^{-3}$	0.51 ± 0.08	0.852	0.57 ± 0.04	-0.64 ± 0.04	19.9 ± 2.0
K/Al = 1.25	0.862	$2.6 \cdot 10^{-1} \pm 2.1 \cdot 10^{-3}$	0 ± 0	0.909	0 ± 0	0.33 ± 0.02	5.0 ± 0.6

[a]k_j was fixed in the eRPM calculations. [b]K/Al ratios of 0.2, 0.5, 1.0, and 1.25 correspond to KOH loadings of 0, 19, 35, and 70 wt %, respectively. [c]Same samples.

conversion and were proportional to the surface areas determined by N_2 adsorption (Table 3). In the nonisothermal CO_2 gasification of SCB char, Edreis et al. suggested that increasing pyrolysis temperatures increased the thermal stability of the carbon structure with a subsequent reduction in the reactivity of the char.[9] The rates were similar to those observed for switchgrass char gasified with CO_2 (maximum of 0.03 min^{-1}),[26] as well as other char gasified with steam including bamboo (maximum of 0.04 min^{-1}), SCB and rice husk (maximum of ~0.02 min^{-1}), and corncob and Hinoki cypress sawdust (maximum of 0.015 min^{-1}).[44] The gasification rates for char samples prepared at temperatures up to 850 °C monotonically decreased with conversion, with the exception of the char sample prepared at 900 °C, which underwent maximum gasification at ~10% conversion. This type of gasification behavior has been previously observed for char materials that, like SCB, have Si as the most abundant ash species.[44,45] As shown in Figure 5a, above 30% conversion, the gasification rates were similar and complete gasification required approximately 140 min for all samples. A time of 50 min was reported for the nonisothermal (with a heating rate of 20 °C min^{-1}) CO_2 gasification of SCB char prepared at 500, 800, and 900 °C but with smaller initial particle sizes in the range of 180−450 μm (compared to the average particle size of 793 μm used herein, Figure 2a) and higher gasification temperatures (up to 1300 °C compared to 850 °C used herein).[9]

After ball milling, the gasification curves were concave down-shaped with maximum rates at ~20% conversion, except for

the char produced at 850 °C, for which the initial rate was the maximum rate (Figure 5b). This sample had the highest surface area (172 m^2/g, Table 3). There was a positive correlation between the initial surface area (as measured by N_2) and the initial gasification rate for all samples (Figure 5d), consistent with gasification in a kinetically controlled regime. Therefore, for samples without KOH, the gasification curves can be interpreted as an indirect measure of porosity and surface area changes. For the char samples as-prepared at 750, 800, or 850 °C, the highest reaction rate occurs at $t = 0$, indicating that the highest porosity existed at the beginning of the process. The gasification curves of the ball-milled samples, however, have a concave shape, which suggests that porosity developed during gasification up to ~20% conversion.

Ball milling reduced the particle sizes (Figure 2c) and porosities (Table 3) while resulting in more oxygen functional groups at the surface (Figure 1 and Table 2). The mass losses during heating to the gasification temperature were higher for the ball-milled samples (11−15 wt % vs 2.6−5.7 wt % for the unmilled samples), consistent with the increased oxygen groups. These groups likely devolatilized and or/reacted with carbon during heating and had a minimal effect on the calculated gasification rates.

Ball milling had the greatest negative impact on the initial gasification rates of char produced at 750 °C (Figure 5a), and so this char was used to test the efficacy of catalyst addition. Char750 was ball milled with different amounts of KOH, and the gasification rates of these mixtures as a function of conversion are shown in Figure 5c, while the particle sizes and
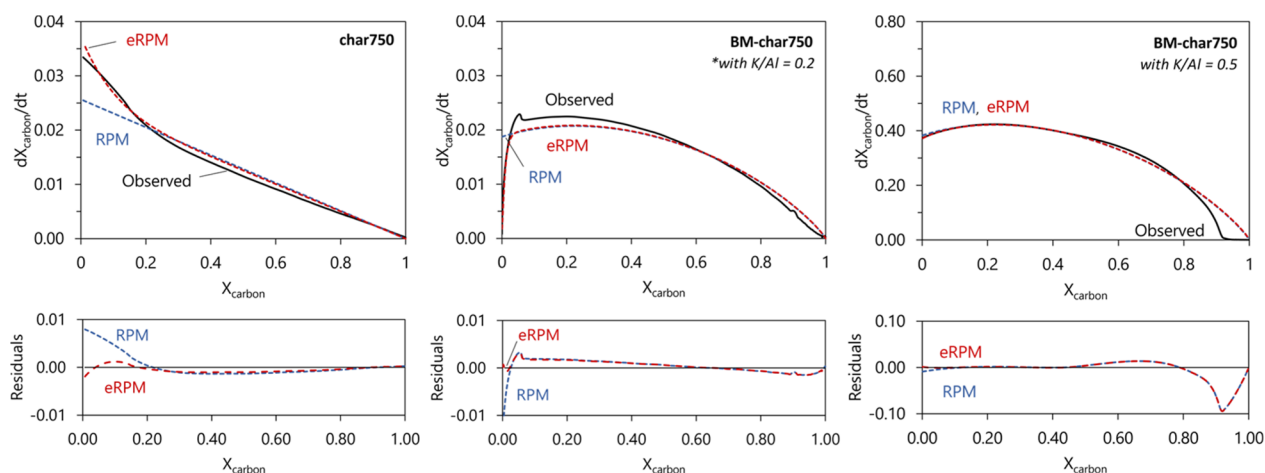
Figure 6. Modeling of the gasification data of char prepared at 750 °C by the RPM and eRPM: fits and residuals. *, same as BM-char750. K/Al = 0.5 (19 wt % KOH loading).

times required to reach 50 and 90% conversion are shown in Table 4. The char samples containing K/Al ratios of 0.5, 1.0, and 1.25 had, respectively, 19-, 30-, and 13-fold increase in the maximum rate compared to the original ball-milled char (with a K/Al ratio of 0.2, Table 2). These maximum rates occurred before 50% conversion, in agreement with previous gasification studies with potassium-catalyzed ash-free carbon black,[46] Genesse raw coal,[47] and switchgrass char.[25,26] The char with a K/Al ratio of 0.5 had a maximum rate at ∼20% conversion, but the rate was relatively constant between 0 and ∼50% conversion. In contrast, the samples with K/Al ratios of 1.0 and 1.25 had more distinct maxima at 30 and 10% conversion, respectively, and, after gasification, the remaining solids (ash including the added K) were stuck to the cooled crucible. For the other samples, the remaining solids were loose in the bottom of the crucible. Other studies with coal have shown that excess K will sinter and block access to CO_2.[47] Inhibition effects with high-catalyst concentrations have also been reported for the gasification of petcoke and SCB with $FeCl_3$ (>7 wt % loading).[11] The pure component-melting temperature of KOH is 406 °C,[48] but K may exist in other forms, including K_2CO_3, leading to complex phase behavior. Another study reported gasification inhibition due to the formation of K silicates.[49]

As shown in Table 4, potassium was located on the particle surfaces after ball milling—the K/Al and K/C ratios calculated using EDX were an order of magnitude higher than that of the target loadings. The sample with a K/Al ratio of 1.0 reached 50% conversion the fastest (0.9 min), but the sample with the K/Al ratio of 0.5 was the fastest to reach 90% conversion—3 min compared to 7 and 21 min for the higher ratios and 60 min with no additional K (Table 4). At the highest two K loadings, the surface K/C ratios were above 0.1, which is the saturation value for K as a catalyst in char gasification, as highlighted in a previous study.[24] Thus, K increased the rate, but at too high loadings, K hindered the gasification.

The RPM and eRPM (eqs 5 and 6) were fit to the gasification data, and these fits were evaluated using model discrimination techniques. The model parameters are shown in Table 5 and representative graphical fits with residuals are shown in Figure 6 (all fits are given in Supporting Information C). The models capture the gasification behavior with one value for the rate constant (k_j) mainly modulated not only by

the carbon conversion level (X_{carbon}) but also by the structural factor (ψ) and two constants (c, p) for the eRPM. The values of k_j followed the same trends as the initial surface areas, as illustrated in Figure 5d (i.e., a higher surface area correlated with a higher rate). The fits for the ball-milled samples, except for the sample prepared at 850 °C, had lower k_j values but higher ψ values, which captured the maxima in the curves. A second char sample was produced at 850 °C, the tests and characterization procedures were repeated, and all results confirmed the outlying behavior. Further investigation, beyond the scope of this paper, is required to determine why ball milling had a different effect on this sample.

Although the correlation coefficients, R^2, were over 0.95 for all but the samples with the two highest amounts of added K, the RPM did not well represent the initial (to ∼20% conversion) gasification behavior of most of the char samples. Using the extended model with the rate constants, k_j, obtained from the RPM, the behavior was more fully represented as depicted in Figure 6 and further shown in Supporting Information C by the lower AIC and relative likelihood (L_k) values, higher Akaike probability share (π_{AIC}),[25,30,47] and more randomly distributed residuals. The determined rate constants for the samples with added K were an order of magnitude higher than those of the other samples. The fit for the sample with a K/Al ratio of 0.5 was very good until a conversion of ∼95%, while the fits were very poor for the highest two levels of K (Table 5 and Supporting Information C). The ψ values were similar for K/Al ratios of 0.2 and 0.5 ($\psi = \sim4$) but significantly smaller for the samples with higher levels of K ($\psi = 0.5$ or 0, respectively), consistent with the excess K increasing the mass-transfer limitations by blocking access of the gasification agent to carbon, and thereby preventing pore formation. The residuals in Figure 6 showed the most deviation from 0 when below 10% and above 80% conversion. The initial behavior is likely not well-represented by the models because of the displacement of N_2 by CO_2 as the reaction gas is introduced, and a variable CO_2 concentration violates a key assumption of the models. The behavior above 80% conversion is likely due to ash sintering at the surface, as the deviation at high conversions is negligible for char750, more significant (∼0.2%) for BM-char750, and much more significant (up to 10%) for BM-char750 with K/Al = 0.5. That

is, the deviation from the model increased with increasing ash content.

Particle size and catalyst addition influence the limiting step in gas−solid processes such as gasification, which may be controlled by mass-transfer limitations (diffusion of mass and heat through the boundary layer around the char particle or through the porous structure) or the gas−solid reactions with the solid surfaces.[50] The extent of transport limitations is usually tested by further increasing either the flow rate of the gasification agent (CO_2) or the feedstock mass in the TGA unit. Both options were not feasible in this study because the system was already operating at the maximum gas flow rate, and increasing the mass of some of the char samples would surpass the maximum feed height in the TGA crucible. Qualitatively, based on the rates and modeling results, gasification of the char samples was likely in a kinetically controlled regime,[51] because the samples had initial particle sizes below 150 μm,[52] the reaction rates were on the order of 10^{-2} min^{-1}, and there was a positive correlation between the initial surface area and the initial gasification rates (Figure 5d). In studies with larger particles—biomass wastes of 0.5−8 mm diameter[53] and wood char from pressed-oil stone of 0.06−2.1 mm[52] diameter—reactivity decreased with particle size because of mass diffusion. When KOH was added to the char samples, the rate increased likely resulting in a mixed kinetic-transport control regime. The sintering of excess K with higher K/Al ratios and/or high levels of conversion further increased the mass-transfer limitations, as highlighted by the decreasing ψ values.

4. CONCLUSIONS

SCB char was prepared, characterized, and then gasified in CO_2 at 850 °C to relate the properties of the char to the gasification reactivity. Pyrolysis between 750 and 900 °C resulted in char materials that had similar morphologies and surface compositions. The porosities, however, were different with decreasing surface area/pore volume as the pyrolysis temperature was increased. Ball milling significantly reduced the particle size by almost two orders of magnitude and resulted in increased oxygen and ash (silicon and aluminum) surface concentrations. The surface areas determined by N_2 adsorption significantly decreased for the char samples prepared at 750 or 800 °C and slightly decreased for the samples prepared at 850 and 900 °C. The gasification rates were positively and linearly correlated with the surface areas, and the behavior was well-modeled by the eRPM. The addition of potassium increased the rates by over an order of magnitude with an optimum level of K/Al ratio between 0.5 and 1 (KOH loadings of 19 and 53 wt %). The gasification behavior was not fully captured by the models at higher potassium loadings likely due to diffusion limitations as the excess K hindered the access of CO_2 to the carbon. These results provide information, regarding the char structure, porosity, and reactivity, for the recirculation of char in a gasifier under similar operating conditions as those used in this study. Namely, char produced at higher temperatures will have a lower porosity and be less reactive, suggesting the optimal operating temperature to be ≤850 °C. Other considerations, such as heating rates, gas composition, and effects of other oxidizing agents (O_2 and steam), however, should also be included in the design of the gasifier. Particle collisions during recirculation may resemble the effects of ball milling, which resulted in size reduction and increased ash and oxygen surface concentrations. Potassium addition increases the initial gasification rates, but K/Al ratios above 0.5−1 hinder gasification at higher conversions..

■ ASSOCIATED CONTENT

ⓢ Supporting Information

The Supporting Information is available free of charge at https://pubs.acs.org/doi/10.1021/acs.energyfuels.0c02786.

EDX data of SCB and char samples; N_2 and CO_2 adsorption characterization of char samples; gasification modeling with the RPM and eRPM (PDF)

■ AUTHOR INFORMATION

Corresponding Author

Josephine M. Hill − *Department of Chemical and Petroleum Engineering, Schulich School of Engineering, University of Calgary, Calgary, Alberta T2N 1N4, Canada;* ◉ orcid.org/0000-0003-2708-565X; Phone: 403-210-9488; Email: jhill@ucalgary.ca; Fax: 403-284-4852

Authors

Ingrid Lopes Motta − *Department of Chemical and Petroleum Engineering, Schulich School of Engineering, University of Calgary, Calgary, Alberta T2N 1N4, Canada;* ◉ orcid.org/0000-0002-1162-931X

Ross A. Arnold − *Department of Chemical and Petroleum Engineering, Schulich School of Engineering, University of Calgary, Calgary, Alberta T2N 1N4, Canada*

Francisco Javier Lopez-Tenllado − *Department of Chemical and Petroleum Engineering, Schulich School of Engineering, University of Calgary, Calgary, Alberta T2N 1N4, Canada*

Rubens Maciel Filho − *Laboratory of Optimization, Design, and Advanced Control, School of Chemical Engineering, University of Campinas, Campinas 13083-852, Brazil*

Maria Regina Wolf Maciel − *Laboratory of Optimization, Design, and Advanced Control, School of Chemical Engineering, University of Campinas, Campinas 13083-852, Brazil*

Complete contact information is available at:
https://pubs.acs.org/10.1021/acs.energyfuels.0c02786

Author Contributions

I.L.M. obtained the SCB samples, prepared the char samples, completed the gasification experiments and modeling, performed most of the characterization, and prepared the manuscript. R.A.A set up the TGA equipment, developed the gasification method, and revised the manuscript. F.J.L.T. performed the N_2 and CO_2 adsorption experiments, FTIR characterization, and revised the manuscript. R.M.F. and M.R.W.M. provided the equipment for proximate and ultimate analyses and revised the manuscript. J.M.H. obtained all the other equipment for characterization and tests, provided project funding, supervised other authors, and revised the manuscript.

Notes

The authors declare no competing financial interest.

■ REFERENCES

(1) Bizzo, W. A.; Lenço, P. C.; Carvalho, D. J.; Veiga, J. P. S. The Generation of Residual Biomass during the Production of Bio-Ethanol from Sugarcane, Its Characterization and Its Use in Energy Production. *Renewable Sustainable Energy Rev.* **2014**, *29*, 589−603.

(2) Hofsetz, K.; Silva, M. A. Brazilian Sugarcane Bagasse: Energy and Non-Energy Consumption. *Biomass Bioenergy* **2012**, *46*, 564−573.

(3) Klasson, K. T. Char from Sugarcane Bagasse. *Biorefinery Co-Products: Phytochemicals, Primary Metabolites and Value-Added Biomass Processing*; Bergeron, C., Carrier, D. J., Ramaswamy, S., Eds.; Wiley: 2012; pp 327−350.

(4) Fan, X.; Yang, L.; Jiang, J. Experimental Study on Industrial-Scale CFB Biomass Gasification. *Renewable Energy* **2020**, *158*, 32−36.

(5) Zhang, C.; Zeng, G.; Huang, D.; Lai, C.; Chen, M.; Cheng, M.; Tang, W.; Tang, L.; Dong, H.; Huang, B.; et al. Biochar for Environmental Management : Mitigating Greenhouse Gas Emissions , Contaminant Treatment , and Potential Negative Impacts. *Chem. Eng. J.* **2019**, *373*, 902−922.

(6) Wang, J.; Wang, S. Preparation, Modification and Environmental Application of Biochar: A Review. *J. Cleaner Prod.* **2019**, *227*, 1002−1022.

(7) Hernández, J. J.; Saffe, A.; Collado, R.; Monedero, E. Recirculation of Char from Biomass Gasification: Effects on Gasifier Performance and End-Char Properties. *Renewable Energy* **2020**, *147*, 806−813.

(8) Edreis, E. M. A.; Luo, G.; Li, A.; Chao, C.; Hu, H.; Zhang, S.; Gui, B.; Xiao, L.; Xu, K.; Zhang, P.; et al. CO2 Co-Gasification of Lower Sulphur Petroleum Coke and Sugar Cane Bagasse via TG−FTIR Analysis Technique. *Bioresour. Technol.* **2013**, *136*, 595−603.

(9) Edreis, E. M. A.; Luo, G.; Yao, H. Investigations of the Structure and Thermal Kinetic Analysis of Sugarcane Bagasse Char during Non-Isothermal CO2 Gasification. *J. Anal. Appl. Pyrolysis* **2014**, *107*, 107−115.

(10) Edreis, E. M. A.; Yao, H. Kinetic Thermal Behaviour and Evaluation of Physical Structure of Sugar Cane Bagasse Char during Non-Isothermal Steam Gasification. *J. Mater. Res. Technol.* **2016**, *5*, 317−326.

(11) Edreis, E. M. A.; Li, X.; Xu, C.; Yao, H. Kinetic Study and Synergistic Interactions on Catalytic CO2 Gasification of Sudanese Lower Sulphur Petroleum Coke and Sugar Cane Bagasse. *J. Mater. Res. Technol.* **2017**, *6*, 147−157.

(12) Edreis, E. M. A.; Li, X.; Luo, G.; Sharshir, S. W.; Yao, H. Kinetic Analyses and Synergistic Effects of CO2 Co-Gasification of Low Sulphur Petroleum Coke and Biomass Wastes. *Bioresour. Technol.* **2018**, *267*, 54−62.

(13) Bhatia, S. K.; Perlmutter, D. D. A Random Pore Model for Fluid-Solid Reactions: I. Isothermal, Kinetic Control. *AIChE J.* **1980**, *26*, 379−386.

(14) Mukherjee, A.; Zimmerman, A. R.; Harris, W. Surface Chemistry Variations among a Series of Laboratory-Produced Biochars. *Geoderma* **2011**, *163*, 247−255.

(15) Ahmad, M.; Lee, S. S.; Dou, X.; Mohan, D.; Sung, J.-K.; Yang, J. E.; Ok, Y. S. Effects of Pyrolysis Temperature on Soybean Stover- and Peanut Shell-Derived Biochar Properties and TCE Adsorption in Water. *Bioresour. Technol.* **2012**, *118*, 536−544.

(16) Zhao, L.; Cao, X.; Mašek, O.; Zimmerman, A. Heterogeneity of Biochar Properties as a Function of Feedstock Sources and Production Temperatures. *J. Hazard. Mater.* **2013**, *256−257*, 1−9.

(17) Gray, M.; Johnson, M. G.; Dragila, M. I.; Kleber, M. Water Uptake in Biochars: The Roles of Porosity and Hydrophobicity. *Biomass Bioenergy* **2014**, *61*, 196−205.

(18) Xu, X.; Zheng, Y.; Gao, B.; Cao, X. N-Doped Biochar Synthesized by a Facile Ball-Milling Method for Enhanced Sorption of CO2 and Reactive Red. *Chem. Eng. J.* **2019**, *368*, 564−572.

(19) Lyu, H.; Gao, B.; He, F.; Zimmerman, A. R.; Ding, C.; Huang, H.; Tang, J. Effects of Ball Milling on the Physicochemical and Sorptive Properties of Biochar: Experimental Observations and Governing Mechanisms. *Environ. Pollut.* **2018**, *233*, 54−63.

(20) Lyu, H.; Gao, B.; He, F.; Zimmerman, A. R.; Ding, C.; Tang, J.; Crittenden, J. C. Experimental and Modeling Investigations of Ball-Milled Biochar for the Removal of Aqueous Methylene Blue. *Chem. Eng. J.* **2018**, *335*, 110−119.

(21) Lyu, H.; Yu, Z.; Gao, B.; He, F.; Huang, J.; Tang, J.; Shen, B. Ball-Milled Biochar for Alternative Carbon Electrode. *Environ. Sci. Pollut. Res.* **2019**, *26*, 14693−14702.

(22) Ferreira, G. F.; Pierozzi, M.; Fingolo, A. C.; da Silva, W. P.; Strauss, M. Tuning Sugarcane Bagasse Biochar into a Potential Carbon Black Substitute for Polyethylene Composites. *J. Polym. Environ.* **2019**, *27*, 1735−1745.

(23) Arnold, R. A.; Hill, J. M. Catalysts for Gasification: A Review. *Sustainable Energy Fuels* **2019**, *3*, 656−672.

(24) Karlström, O.; Dirbeba, M. J.; Costa, M.; Brink, A.; Hupa, M. Influence of K/C Ratio on Gasification Rate of Biomass Chars. *Energy Fuels* **2018**, *32*, 10695−10700.

(25) Arnold, R. A.; Habibi, R.; Kopyscinski, J.; Hill, J. M. Interaction of Potassium and Calcium in the Catalytic Gasification of Biosolids and Switchgrass. *Energy Fuels* **2017**, *31*, 6240−6247.

(26) Habibi, R.; Kopyscinski, J.; Masnadi, M. S.; Lam, J.; Grace, J. R.; Mims, C. A.; Hill, J. M. Co-Gasification of Biomass and Non-Biomass Feedstocks: Synergistic and Inhibition Effects of Switchgrass Mixed with Sub-Bituminous Coal and Fluid Coke During CO2 Gasification. *Energy Fuels* **2013**, *27*, 494−500.

(27) Venderbosch, R. H.; Prins, W. Fast Pyrolysis. *Thermochemical Processing of Biomass: Conversion into Fuels, Chemicals and Power*; Brown, R. C., Ed.; John Wiley & Sons: Chichester, 2011; pp 124−156. DOI: DOI: 10.1002/9781119990840.ch5.

(28) Edreis, E. M. A.; Luo, G.; Li, A.; Xu, C.; Yao, H. Synergistic Effects and Kinetics Thermal Behaviour of Petroleum Coke/Biomass Blends during H2O Co-Gasification. *Energy Convers. Manage.* **2014**, *79*, 355−366.

(29) Bhatia, S. K.; Vartak, B. J. Reaction of Microporous Solids: The Discrete Random Pore Model. *Carbon* **1996**, *34*, 1383−1391.

(30) Kopyscinski, J.; Habibi, R.; Mims, C. A.; Hill, J. M. K2CO3−Catalyzed CO2 Gasification of Ash-Free Coal: Kinetic Study. *Energy Fuels* **2013**, *27*, 4875−4883.

(31) de Medeiros, E. M.; Posada, J. A.; Noorman, H.; Osseweijer, P.; Filho, R. M. Hydrous Bioethanol Production from Sugarcane Bagasse via Energy Self-Sufficient Gasification-Fermentation Hybrid Route: Simulation and Financial Analysis. *J. Cleaner Prod.* **2017**, *168*, 1625−1635.

(32) Hernández, C.; Escamilla-Alvarado, C.; Sánchez, A.; Alarcón, E.; Ziarelli, F.; Musule, R.; Valdez-Vazquez, I. Wheat Straw, Corn Stover, Sugarcane, and Agave Biomasses: Chemical Properties, Availability, and Cellulosic-Bioethanol Production Potential in Mexico. *Biofuels, Bioprod. Biorefin.* **2019**, *13*, 1143−1159.

(33) Asadullah, M. Biomass Gasification Gas Cleaning for Downstream Applications: A Comparative Critical Review. *Renewable Sustainable Energy Rev.* **2014**, *40*, 118−132.

(34) Tahiri, N.; Khouchaf, L.; Elaatmani, M.; Louarn, G.; Zegzouti, A.; Daoud, M. Study of the Thermal Treatment of SiO2 Aggregate. *IOP Conf. Ser.: Mater. Sci. Eng.* **2014**, *62*, 27−29.

(35) Nebra, S. A.; de C.Macedo, I. Bagasse Particles Shape and Size and Their Free-Settling Velocity. *Int. Sugar J.* **1987**, *90*, 168−170.

(36) Wu, R.; Beutler, J.; Price, C.; Baxter, L. L. Biomass Char Particle Surface Area and Porosity Dynamics during Gasification. *Fuel* **2020**, *264*, 116833.

(37) Das, O.; Sarmah, A. K.; Bhattacharyya, D. Structure-Mechanics Property Relationship of Waste Derived Biochars. *Sci. Total Environ.* **2015**, *538*, 611−620.

(38) Wallace, C. A.; Saha, G. C.; Afzal, M. T.; Lloyd, A. Experimental and Computational Modeling of Effective Flexural/Tensile Properties of Microwave Pyrolysis Biochar Reinforced GFRP Biocomposites. *Composites, Part B* **2019**, *175*, 107180.

(39) Wallace, C. A.; Afzal, M. T.; Saha, G. C. Effect of Feedstock and Microwave Pyrolysis Temperature on Physio-Chemical and Nano-Scale Mechanical Properties of Biochar. *Bioresour. Bioprocess.* **2019**, *6*, 33.

(40) Zickler, G. A.; Schöberl, T.; Paris, O. Mechanical Properties of Pyrolysed Wood: A Nanoindentation Study. *Philos. Mag.* **2006**, *86*, 1373−1386.

(41) MEMSnet. Material: Silicon Dioxide (SiO2). bulk https://www.memsnet.org/material/silicondioxidesio2bulk/ (accessed August 17, 2020).

(42) Rouquerol, J.; Llewellyn, P.; Rouquerol, F. Is the BET Equation Applicable to Microporous Adsorbents? *Stud. Surf. Sci. Catal.* **2007**, *160*, 49−56.

(43) Angın, D. Effect of Pyrolysis Temperature and Heating Rate on Biochar Obtained from Pyrolysis of Safflower Seed Press Cake. *Bioresour. Technol.* **2013**, *128*, 593−597.

(44) Zhang, Y.; Ashizawa, M.; Kajitani, S.; Miura, K. Proposal of a Semi-Empirical Kinetic Model to Reconcile with Gasification Reactivity Profiles of Biomass Chars. *Fuel* **2008**, *87*, 475−481.

(45) Romero Millán, L. M.; Sierra Vargas, F. E.; Nzihou, A. Catalytic Effect of Inorganic Elements on Steam Gasification Biochar Properties from Agrowastes. *Energy Fuels* **2019**, *33*, 8666−8675.

(46) Arnold, R. A.; Hill, J. M. Effect of Calcium and Barium on Potassium-Catalyzed Gasification of Ash-Free Carbon Black. *Fuel* **2019**, *254*, 115647.

(47) Islam, S.; Kopyscinski, J.; Liew, S. C.; Hill, J. M. Impact of K2CO3 Catalyst Loading on the CO2-Gasification of Genesse Raw Coal and Low-Ash Product. *Powder Technol.* **2016**, *290*, 141−147.

(48) Haynes, W. *CRC Handbook of Chemistry and Physics*; 95th ed.; Haynes, W., Ed.; CRC Press LLC: Boca Raton, 2014.

(49) Strandberg, A.; Holmgren, P.; Wagner, D. R.; Molinder, R.; Wiinikka, H.; Umeki, K.; Broström, M. Effects of Pyrolysis Conditions and Ash Formation on Gasification Rates of Biomass Char. *Energy Fuels* **2017**, *31*, 6507−6514.

(50) Laurendeau, N. M. Heterogeneous Kinetics of Coal Char Gasification and Combustion. *Prog. Energy Combust. Sci.* **1978**, *4*, 221−270.

(51) Adschiri, T.; Furusawa, T. Relation between CO2-Reactivity of Coal Char and BET Surface Area. *Fuel* **1986**, *65*, 927−931.

(52) Gómez-Barea, A.; Ollero, P.; Fernández-Baco, C. Diffusional Effects in CO2 Gasification Experiments with Single Biomass Char Particles. 1. Experimental Investigation. *Energy Fuels* **2006**, *20*, 2202−2210.

(53) Hernández, J. J.; Aranda-Almansa, G.; Bula, A. Gasification of Biomass Wastes in an Entrained Flow Gasifier: Effect of the Particle Size and the Residence Time. *Fuel Process. Technol.* **2010**, *91*, 681−692.